Proceedings of the ASME 2020
International Mechanical Engineering Congress and Exposition
IMECE2020
November 16-19, 2020, Portland, OR, USA

IMECE2020-23322

ACCELERATING LARGE-FORMAT METAL ADDITIVE MANUFACTURING: HOW CONTROLS R&D IS DRIVING SPEED, SCALE, AND EFFICIENCY

Brian T. Gibson[1], Paritosh Mhatre, Michael C. Borish, Justin L. West, Emma D. Betters, Scott S. Smith, Bradley S. Richardson, Lonnie J. Love
Manufacturing Demonstration Facility
Oak Ridge National Laboratory
Knoxville, TN, USA

Tayler W. Sundermann
University of Nebraska, Lincoln, NE, USA

John T. Potter, Emma J. Vetland, William C. Henry, Christopher P. Allison
GKN Aerospace, USA, St. Louis, MO, USA

ABSTRACT

This article highlights work at Oak Ridge National Laboratory's Manufacturing Demonstration Facility to develop closed-loop, feedback control for laser-wire based Directed Energy Deposition, a form of metal Big Area Additive Manufacturing (m-BAAM), a process being developed in partnership with GKN Aerospace specifically for the production of Ti-6Al-4V pre-forms for aerospace components. A large-scale structural demonstrator component is presented as a case-study in which not just control, but the entire 3D printing workflow for m-BAAM is discussed in detail, including design principles for large-format metal AM, toolpath generation, parameter development, process control, and system operation, as well as post-print net-shape geometric analysis and finish machining. In terms of control, a multi-sensor approach has been utilized to measure both layer height and melt pool size, and multiple modes of closed-loop control have been developed to manipulate process parameters (laser power, print speed, deposition rate) to control these variables. Layer height control and melt pool size control have yielded excellent local (intralayer) and global (component-level) geometry control, and the impact of melt pool size control in particular on thermal gradients and material properties is the subject of continuing research. Further, these modes of control have allowed the process to advance to higher deposition rates (exceeding 7.5 lb/hr), larger parts (1-meter scale), shorter build times, and higher overall efficiency. The control modes are examined individually, highlighting their development, demonstration, and lessons learned, and it is shown how they operate concurrently to enable the printing of a large-scale, near net shape Ti-6Al-4V component.

Keywords: Additive Manufacturing, 3D Printing, Metal, Control

NOMENCLATURE

AM	additive manufacturing
DED	directed energy deposition
DP	deposition rate
HWP	hot wire power
LH	layer height
LP	laser power
m-BAAM	metal Big Area Additive Manufacturing
ORNL	Oak Ridge National Laboratory
PS	print speed

1. INTRODUCTION

Large-format metal additive manufacturing (AM), also known as metal Big Area Additive Manufacturing (m-BAAM), is poised to be a disruptive technology in several sectors, including the tool and die and aerospace industries, where high costs and long lead times associated with metallic components are the driving factors toward a change from conventional methods of manufacturing. The challenge of large-format metal additive manufacturing, however, is simultaneous control of geometry, material properties, and residual stress and distortion

[1] Contact author: gibsonbt@ornl.gov

[1]. Along with pre-print modeling and simulation and post-print characterization, real-time sensing and closed-loop control have become important tools in addressing this challenge. The capability to sense build geometry and thermal properties in real-time means that systems can react automatically to compensate for changing geometric and thermal conditions as they arise, taking significant front-end workload off the AM user with respect to modeling and process planning. It also means that in addition to mass production, low-volume production runs of custom components are possible in rapid-turnaround development cycles.

Because of the aforementioned benefits, and because of the impact deposition conditions have on the resulting material properties in a build [2-4], control of metal AM processes has garnered much attention from the R&D community in recent years [5], from powder-based processes to large-scale wire-fed processes. Heralic et al. [6] have been significant contributors in the area of sensor development and process control in laser-wire deposition, as have been Nassar et al. in powder-based processes [7]. Specifically in terms of melt pool size control, there have been a few examples of closed-loop control, as opposed to modeling or feed-forward control approaches, including Hofmeister et al. [8] and Hu et al. [9] in laser powder-based DED processes, Hu et al. in laser cladding [10], and Zalameda et al. [11] in an electron beam freeform fabrication process. The present authors have engaged in a significant R&D effort to develop multiple forms of process control for a laser hot-wire DED or m-BAAM process for the net-shape deposition of Titanium. Efforts have yielded advancements in layer height control [12], melt pool monitoring [13], integration of multiple forms of thermal control, including real-time closed-loop melt pool size control [14], and site-specific control [15], a novel methodology which seeks to tailor deposition characteristics on a location-specific basis. While the effort to develop these capabilities was robust, a case study was needed to examine the cumulative effects of concurrent operation of all of the control algorithms together. In the work presented here, a large-scale m-BAAM demonstrator part was printed as a means for testing these recently developed process control techniques. These techniques include layer height control and multiple modes of thermal control: real-time closed-loop melt pool size control and layer-wise average laser power control. The use of these modes of control have numerous impacts, including dynamically increasing deposition rates, leading to shorter build times and higher overall efficiency.

2. MATERIALS AND METHODS

The methods used to print a large-scale (1 m long) demonstrator part in Ti-6Al-4V are the combination of the best practices learned over the course of an extensive R&D effort focused on developing this m-BAAM process, including parameter development, which also involves hot-wire optimization for increasing deposition rates, design for additive, tool path generation, real-time process control, including height control and multiple modes of thermal control, and system operation. The multiple forms of process control are considered the key-enablers highlighted here, but other aspects are discussed as well, including net-shape analysis and post-print machining.

The demonstrator part was printed in a large-scale, custom deposition cell, the heart of which is a 6-axis industrial robot. Subsystems include the lasers (2 10kW fiber-delivered diode lasers feeding into a combiner), chillers, wirefeeder (1.6 mm diameter Ti-6Al-4V wire was the feedstock), Argon control and soot collection for maintaining the deposition environment (below 300 ppm O_2 during deposition), and sensor systems. The sensor systems, which include a laser line scanner and an in-axis thermal camera, and which are obviously central to enabling feedback control, are discussed in further detail in subsequent sections.

2.1 Parameter Development

Parameter development mainly deals with the selection of primary process variables (laser power, print speed, and deposition rate) for achieving process stability and the desired deposition characteristics. One of the goals associated with the demonstrator part was to achieve not just scale (1 m), but also significantly higher deposition rates compared to what is considered typical for m-BAAM with Titanium (instantaneous deposition rates of on the order of 1.8 - 2.4 kg/hr). First, in order to achieve significantly higher deposition rates, a study was carried out that examined the possibility of increasing the power contribution from the hot wire system, which provides auxiliary, resistance heating to the wire before it enters the melt pool. Hot wire is advantageous in that it has a higher thermal transfer efficiency from the heat source to the substrate than the laser, which is subject to reflection. A series of walls was printed with varying combinations of deposition rates and hot wire power levels that yielded stable processes. Through this investigation, it was found that a 3.58 kg/hr nominal (instantaneous) deposition rate was achievable with 820 W of hot wire power, even while maintaining delivered laser power at a relatively low nominal level of 8.71 kW. The primary process parameters selected for the demonstrator part are shown in Table 1. These are considered only the nominal parameters since laser power, deposition rate, and print speed can all be modulated by process control algorithms during the printing of parts.

TABLE 1: NOMINAL DEPOSITION PARAMETERS

Parameter	Value	Units
Laser Power (LP)	8.71	kW
Hot Wire Power (HWP)	820	W
Deposition Rate (DP)	3.58	kg/hr
Print Speed (PS)	8	mm/s
Layer Height (LH)	2.4	mm

2.2 Design for m-BAAM

The design selected for the demonstrator was a thin-walled airfoil with pass-throughs, in a nod to the aerospace industry partnership with GKN Aerospace, and to highlight process capabilities for depositing complex geometries with overhangs. The demonstrator CAD model is shown in Figure 1.

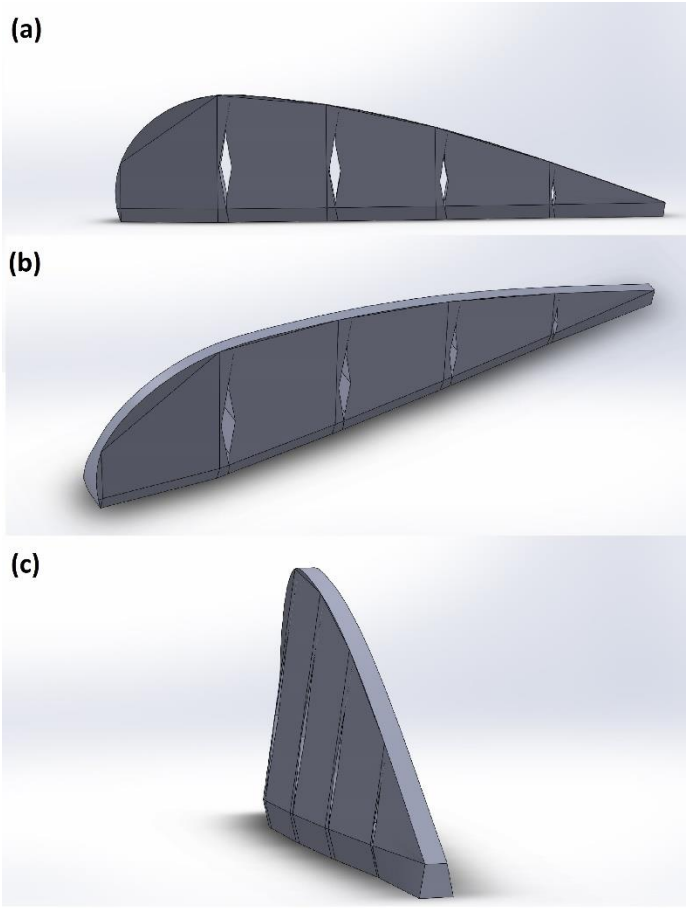

FIGURE 1: AIRFOIL DESIGN: SIDE VIEW (a), FRONT ISO VIEW (b), BACK ISO VIEW (c)

The length of the component is 1 m at its base, meaning 1 m is exceeded as the part flares outward in the initial layers before tapering inward; the part height is approximately 230 mm. There are five hollow sections of single-bead thickness, with the exception of the regions where sections merge, in which bead overlap essentially creates sections of double-bead walls. The beads of the double-bead walls deviate to form the pass-throughs before re-merging near the top curvature of the part. This is a unique geometry that highlights the value of m-BAAM; it would be difficult, if not impossible, to replicate the component using other manufacturing techniques.

Other unique attributes of the part include that it is comprised almost entirely of 10° overhangs and that it is a modular design (5 sections), lacking a perimeter bead, that yielded a monolithic structure when printed, due to the fusing of neighboring sections, a possibility for m-BAAM that would typically not be a viable design option for polymer-based materials and systems. Visible in the CAD model in Figure 1 are tiny cuts that extend from the top and bottom of the pass-throughs; these were placed in the model to facilitate the desired toolpath (5 sections of closed-contours) during slicing.

2.3 Toolpath Generation

Tool pathing was carefully considered for this part. The ORNL Slicer was used for toolpath and machine code generation, and this slicer has been developed over the course of this R&D effort to include tailored capabilities for m-BAAM pathing. This includes control over rotation or randomization of bead start/stop points on a per layer basis and reversal of the direction of perimeter/inset printing on a per layer basis. These options have the impact of better maintaining nominal layer height and wall thickness by washing out the effects of height deviations at bead initiation or termination points and wire feed directionality-dependent bead width. These options were used for the printing of this part. Figure 2 shows the pathing for layers 1 and 2 of the part, with the bead start/stop points indicated. The conventions of layers 1 and 2 were continued for all odd and even numbered layers, respectively. For odd numbered layers, the travel direction around each closed-contour path was counterclockwise, and for even numbered layers clockwise.

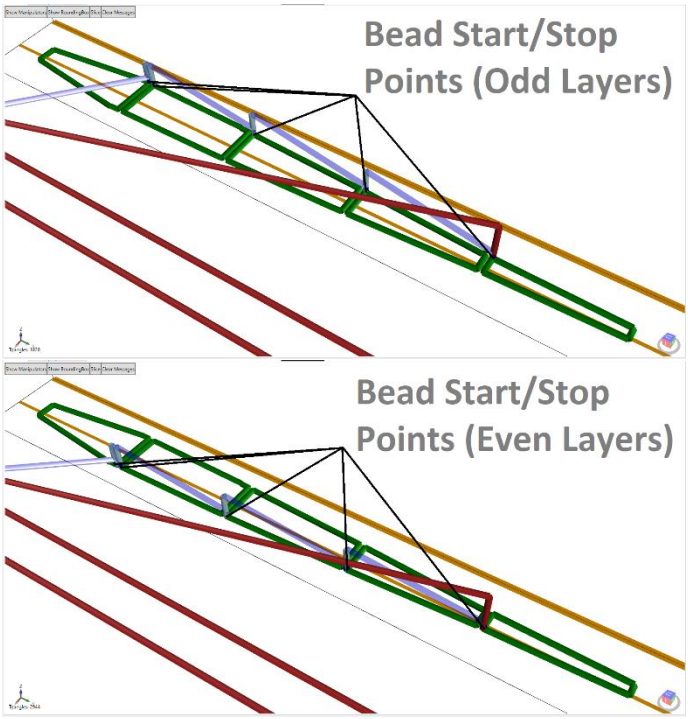

FIGURE 2: TOOLPATH IN THE SLICER SHOWING BEAD START POINTS: ODD NUMBERED LAYERS (TOP), EVEN NUMBERED LAYERS (BOTTOM)

Looking at the individual layers, as in Figure 2, and the combined pathing for the entire part, as in Figure 3, it can clearly be seen how the tiny cuts in the CAD model facilitated the desired pathing. Also, in Figure 3, it can be seen that the upper cuts end before reaching the top of the part, allowing for brief intralayer tie-in of the neighboring sections.

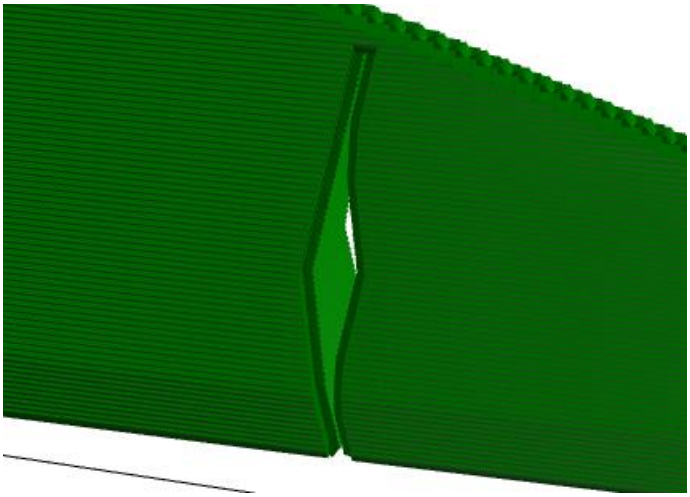

FIGURE 3: CLOSE-UP OF TOOLPATHS IN THE SLICER SHOWING A PASSTHROUGH AND SECTION RE-JOINING ABOVE IT

2.4 Process Control

Process control has been developed significantly over the course of this R&D effort. It now includes height control and multiple modes of thermal control operating concurrently. Thermal control includes two control loops, one in which melt pool size is controlled in real-time, and another in which average laser power is controlled on a per layer basis.

2.5 Height Control

Height control utilizes the laser line scanner that is mounted to the print head to scan the deposited geometry, which is compared against the ideal representation of the geometry determined in the slicing process.

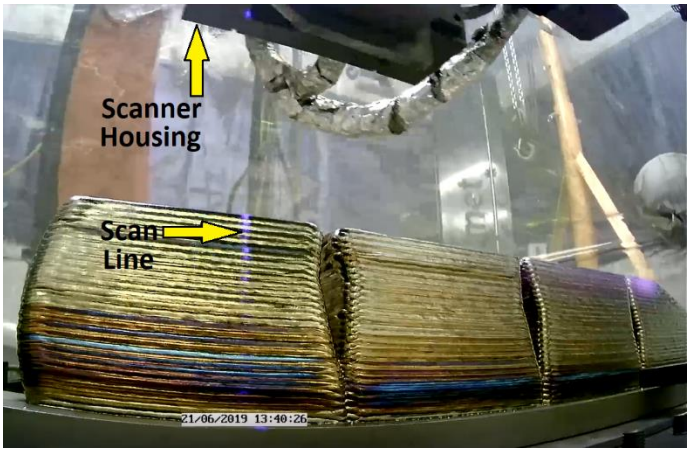

FIGURE 4: IMAGE CAPTURE FROM A CELL CAMERA SHOWING THE SCAN LINE PROJECTION ONTO THE PART

Deviations from the ideal geometry then drive modifications to deposition rate, relative to the layer nominal deposition rate, on the next layer to correct geometry defects.

2.6 Real-Time Melt Pool Size Control

The in-axis thermal camera provides an image of the melt pool, an example of which is shown in Figure 5, from which features, i.e. melt pool size, width, length can be extracted in real-time. The most frequently used control mode and the one utilized for printing the demonstrator is one in which laser power is modulated in real-time to control melt pool size, which yields a fine, intralayer control of geometry and impacts thermal gradients as well; the effect on thermal gradients and heating and cooling rates is a subject of continuing research.

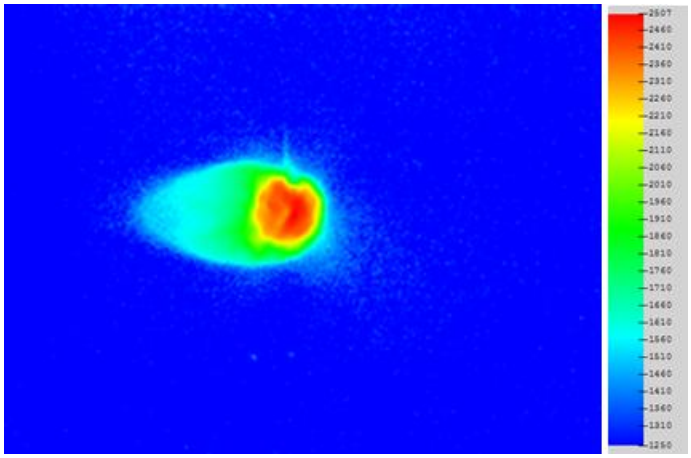

FIGURE 5: MELT POOL IMAGE FROM IN-AXIS THERMAL CAMERA; SCALE UNITS ARE IN DEGREES CELSIUS

There is also a coarse, interlayer effect associated with melt pool size control, which is a decrease in average laser power as heat accumulates in the component under construction. From a production efficiency standpoint, this is not desired, so the second form of thermal control utilized here is average laser power control.

2.7 Average Laser Power Control

Average laser power control modulates print speed and deposition rate on a per layer basis to prevent power decreases and use the accumulated heat in the component under construction to maintain process stability as print speed and deposition rate increase; or stated more simply, as the part heats up, it is possible to print faster, and printing faster is desired, rather than allowing laser power to decease under closed-loop melt pool size control. The ratio of deposition rate to print speed is maintained as they are modulated to maintain the amount of material deposited per unit length and thus bead geometry. Utilization of both height control, which manipulates deposition rate within the layer, and this second form of thermal control, which manipulates the layer nominal deposition rate, mean that for the demonstrator component, deposition rates increased well beyond the 3.58 kg/hr nominal rate.

2.8 System Operation

System operation includes several aspects, some of which are often overlooked in terms of their importance, that when executed well, can lead to successful prints that require little-to-no operator intervention during deposition, and when executed poorly, can lead to unstable deposition characteristics and even failed prints. These aspects include, but are not limited to:

- Teaching the robot base, which is the virtual representation of the build plate position and orientation
- Determining the deposition and scan orientations of the print head and inputting the information into the slicer
- Setting and maintaining the wire input location, relative to the melt pool (critical for process stability)
- Setting the wirefeeder drive tension; some allowable slippage can prevent drive over-torqueing and tripping
- Periodic changeout or cleaning of wirefeeder tips

These aspects are critical to successful system operation and flawless execution of prints.

2.9 Geometric Net-Shape Analysis

After printing, the demonstrator part was scanned with a FaroARM scanner to create a 3D digital representation of the part, which could be compared against the original CAD model to conduct a net-shape analysis and also assess viability of machining plans.

2.10 Post-Print Machining

After heat treatment, a section of the part and the build plate were machined to highlight the complexity of the build, specifically to create openings in the hollow sections to clearly show that it is a thin-walled structure. The machining model concept is shown in Figure 6. Machining would also make the monolithic, continuous structure created by the modular approach conspicuous after removing the surface texture.

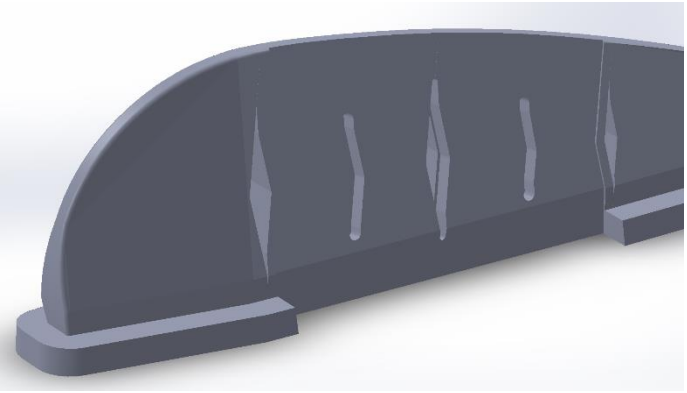

FIGURE 6: MACHING MODEL FOR AIRFOIL INCLUDING BASEPLATE TRIMMING WITH WATERJET

3. RESULTS AND DISCUSSION

The demonstrator component is shown under construction at two stages in Figure 7. Each subsection is hollow and closes and merges together with the next subsection in a sequential manner from the ‘tail’ of the part.

FIGURE 7: PRINTING PROGRESS: LAYER 29 OF 97 (TOP), LAYER 61 OF 97 (BOTTOM)

The completed demonstrator is shown in Figure 8; it required 12.1 hours to print, weighed 17.6 kg (38.9 lb) and consisted of 97 layers and 376 individual beads (closed contours).

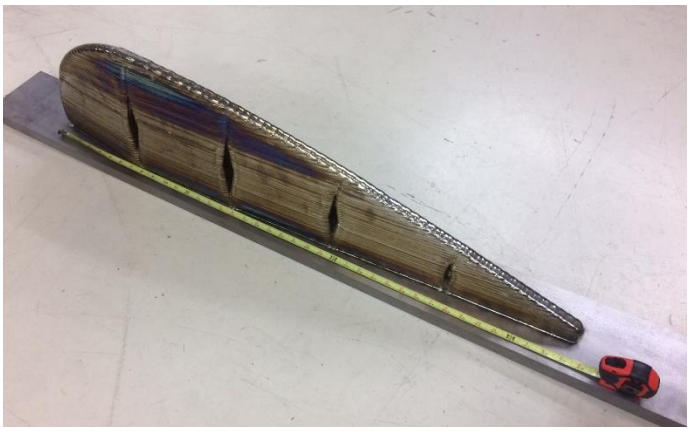

FIGURE 8: COMPLETED DEMONSTRATOR PART WITH INCH SCALE SHOWN

The deposition rate was analyzed on a per bead basis, and the nominal command, bead average, and peak instantaneous deposition rates are plotted in Figure 9.

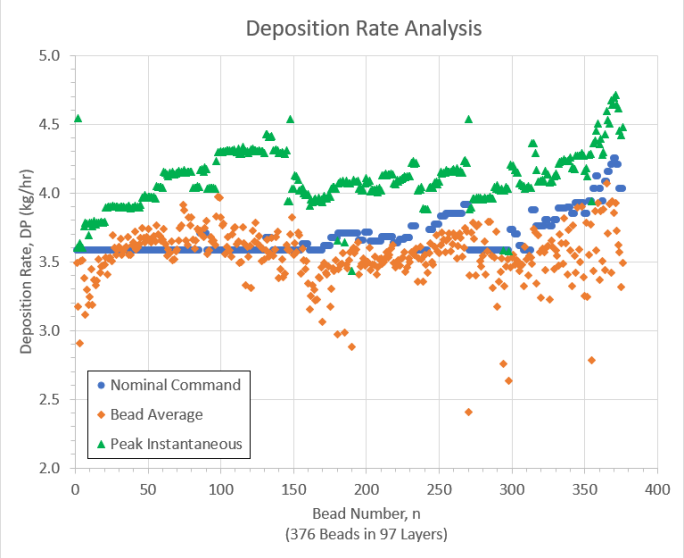

FIGURE 9: BEAD-BASED DEPOSITION RATE ANALYSIS

Because of the process control algorithms being utilized, fine changes to deposition rate occur continuously within a bead, and coarse changes can occur on a layer-to-layer basis. The fine variations are driven by the height control algorithm, and the coarse variations are driven by average laser power control. The nominal command can be thought of as the base deposition rate for a bead; for the demonstrator, the initial, nominal command was 3.58 kg.hr. This rate could vary upward from there, depending on the thermal properties of the part under construction. As the part heats up, and less laser power is required to achieve the desired melt pool size, the system automatically increases print speed and deposition rate in proportion to maintain laser power (and increase process efficiency); this is the functionality of average laser power control, which leads to coarse changes in deposition rate on a layer-by-layer basis. This behavior is evident in the nominal command data shown in Figure 9 in sessions 2 and 3 of the print (the demonstrator was printed over the course of 3 sessions, between which the part cooled to room temperature, which is evident as a distinct periodicity in the deposition rate data, caused by thermal cycling of the build). This behavior is evident only in sessions 2 and 3 because of the unique design of the part. In the initial layers, printing was spread out over a 1 m long cross-section, leading to less heat build-up, but the cross-section decreases in size as printing progresses. The nominal command increased to a maximum of 4.25 kg/hr from 3.58 kg/hr.

The fine variations in deposition rate driven by height control, within each individual bead, occur relative to the nominal deposition rate command for the particular layer being printed, thus there is a stacking effect of the control algorithms (average laser power control, then height control) that impact deposition rate. Height control involves scanning of the build geometry; as printing of the subsequent layer occurs, the height data is used to drive changes to the deposition rate, e.g. increase deposition rate in low spots, decrease deposition rate in high spots, etc. to control layer height. Thus, deposition rate varies continuously during the deposition of a bead; and therefore, the bead average was calculated to capture a statistical measure of the deposition rate for each bead. The bead average is plotted in Figure 9, along with the peak instantaneous rate, which is the maximum deposition rate that occurred within each bead. An interesting observation is that both the bead average and the peak instantaneous rate tended to increase throughout each of the 3 printing sessions, behavior that is not unexpected. This is due to the fact that as a print is initiated and the substrate is at room temperature, beads tend to deposit slightly taller than layer height and later decrease to at or below layer height due to heat accumulation. The observed upward trend in deposition rates is reflective of the actions of height control to react to this phenomenon. Finally, the overall deposition rate statistics for the demonstrator are summarized in Table 2.

TABLE 2: DEPOSITION STATISTICS

Total Print Time	12.1	hours			
Part Length	1	m			
Part Weight	17.6	kg		38.9	lb
Deposition Rates:					
Nominal Command	3.58 - 4.25	kg/hr		7.89 - 9.37	lb/hr
Overall Bead Average	3.55	kg/hr		7.84	lb/hr
Highest Individual Bead Average	4.07	kg/hr		8.97	lb/hr
Peak Instantaneous	4.71	kg/hr		10.38	lb/hr
Session (net)	1.46	kg/hr		3.22	lb/hr

The overall bead average of 3.55 kg/hr is an average of the individual bead averages that were plotted in Figure 9. The highest individual bead average was 4.07 kg/hr. And, the peak instantaneous deposition rate of 4.71 kg/hr was the maximum individual peak instantaneous rate plotted in Figure 9. The session or net deposition rate reflects the total print time, including down time between depositing for actions such as wire-cuts or planned cooling time.

Net-shape analysis for the demonstrator is shown in Figure 10. Overall, the net-shape of the deposited component matched the CAD model very well.

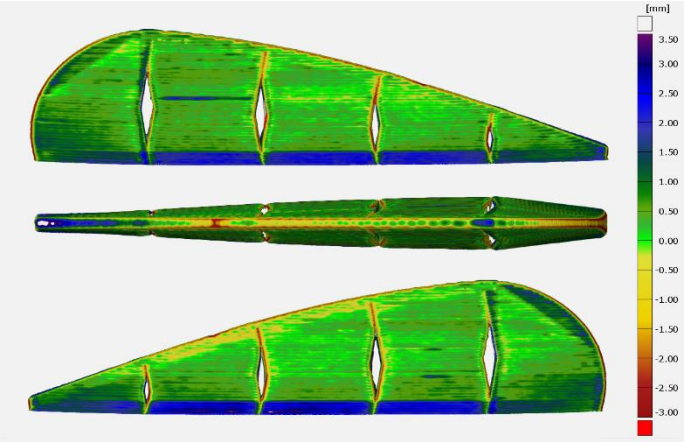

FIGURE 10: NET-SHAPE ANALYSIS: COMPARISON OF CAD MODEL AND FAROARM SCAN OF COMPLETED PART

Deviations were likely driven by a few different factors. In the initial layers, the melt pool size control set-point was intentionally increased beyond nominal (up to +30%) to aid in the deposition of the first layers on the room-temperature build plate (higher than normal laser powers can be beneficial in this regime from a deposition stability perspective); this, along with an outward 10° wall angle, likely contributed to the bulge of material beyond the CAD model in the region. Secondly, build plate and bulk component distortion likely contributed to the deviations along the top arc of the component.

After printing, the component was sent out for heat treatment (stress relieve) at a GKN facility. Figure 11 shows the demonstrator after heat treatment. Most of the surface oxides were removed, but a significant amount of distortion remained.

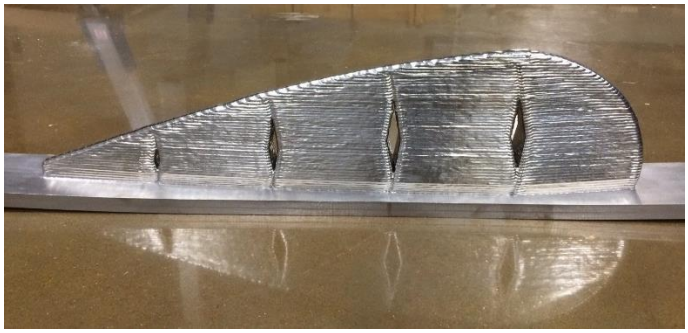

FIGURE 11: DEMONSTRATOR AFTER HEAT-TREATMENT; SURFACE OXIDES HAVE MOSTLY BEEN REMOVED

Machining was conducted on a HAAS VF-5 vertical mill. A notable challenge was determining cutting parameters since the part was much less stiff than the tool. The stiffness of the setup and lack of coolant in the machine significantly increased the overall machining time. The planned depth of cut is shown in Figure 12.

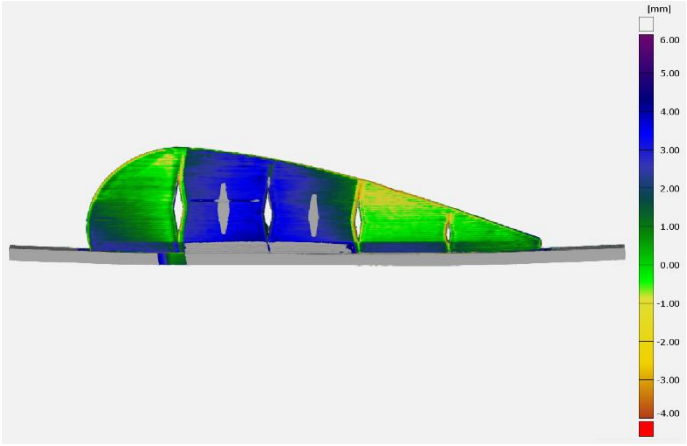

FIGURE 12: PLANNED DEPTH-OF-CUT BASED ON THE MACHINING MODEL AND THE FAROARM SCAN OF THE COMPLETED PART

Usually finding the print is a challenge, but in this case the build was centered well on the build plate and, as it was a demonstration rather than production part, it did not require tight dimensional accuracy. A double angle fixture plate made aligning the part straightforward and the diamond-shaped pass-throughs provided a reliable symmetric reference. The total machining time was 12.5 hours with a tooling cost of $500 and a consumable fixture cost of $200. The machined demonstrator (prior to base plate water-jetting) is shown in Figure 13.

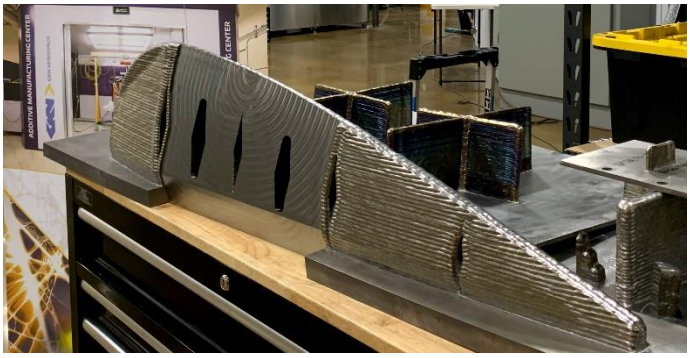

FIGURE 13: DEMONSTRATOR AFTER MACHINING, BEFORE BASEPLATE WATER-JETTING

4. CONCLUSION

A Ti-6Al-4V demonstrator part was printed using a laser-wire m-BAAM process as means to test multiple process control algorithms and evaluate their ability to facilitate larger-scale printing, higher deposition rates, and increased process efficiency. A 1 m long, 17.6 kg (38.9 lb), geometrically complex demonstrator was printed in 12.1 hours, and instantaneous deposition rates dynamically exceeded 4.5 kg/hr (9.9 lb/hr) due to the process control algorithms implemented, achieving at times, a greater than 30% improvement in process efficiency with no direct intervention from the operator. Success depended on not just process control however, but numerous factors that were summarized here, including:

- Parameter development
- Design for m-BAAM
- Toolpath generation
- Process control
- System operation

The importance of additional post-printing processes, such as net-shape analysis and machining, were covered as well. All of these aspects must be considered in the development of a well-designed production process based around large-scale metal additive manufacturing.

ACKNOWLEDGEMENTS

This research was funded by the U.S. Department of Energy, Office of Energy Efficiency and Renewable Energy, Advanced Manufacturing Office in partnership with GKN Aerospace. The authors would also like to acknowledge the contributions of the broader Oak Ridge National Laboratory and GKN Aerospace teams, including Alex Roschli and Brian Post of ORNL, and Aaron Thornton and Jeremy Tylenda of GKN Aerospace.

REFERENCES

[1] Suresh S. Babu, Lonnie J. Love, Ryan Dehoff, William H. Peter, Thomas R. Watkins, and S. Pannala. “Additive Manufacturing of Materials: Opportunities and Challenges.” *MRS Bulletin* Vol. 40 (2015): pp. 1154 - 1161. DOI 10.1557/mrs.2015.234.

[2] Lewandowski, J.J., Seifi, M., “Metal Additive Manufacturing: A Review of Mechanical Properties.” *Annu. Rev. Mater. Res.* Vol. 46 (2016): pp. 151 - 86.

[3] Collins, P.C., Brice, D.A., Samimi, P., Ghamarian, I., Fraser, H.L., “Microstructural Control of Additively Manufactured Materials.” *Annu. Rev. Mater. Res.* Vol. 46 (2016): pp. 63 - 91.

[4] Seifi, M., Salem, A., Beuth, J., Harrysson, O., Lewandowski, J.J., “Overview of Materials Qualification Needs for Metal Additive Manufacturing.” *JOM* Vol. 68 No. 3 (2016): pp. 747 - 64.

[5] Donghong Ding, Zengxi Pan, Dominic Cuiuri, and Huijun Li. “Wire-feed additive manufacturing of metal components: technologies, developments and future interests.” *Int J Adv Manuf Technol* Vol 81 (2015): pp. 465 - 481. DOI 10.1007/s00170-015-7077-3.

[6] A. Heralic, A.K. Christiansson, K. Hurtig, M. Ottosson, B. Lennartson. “Control design for automation of robotized laser metal-wire deposition.” *Proceedings of the 17th World Congress of The International Federation of Automatic Control*, Seoul, Korea, July 6 - 11, 2008.

[7] Abdalla R. Nassar, Edward W. Reutzel, Stephen W. Brown, John P. Morgan, Jacob P. Morgan, Donald J. Natale, Rick L. Tutwiler, David P. Feck, and Jeffery C. Banks. “Sensing for directed energy deposition and powder bed fusion additive manufacturing at Penn State University.” *Proceedings of SPIE - The International Society for Optical Engineering*, Vol 9738, Presented at Laser 3D Manufacturing III, San Francisco, CA, Feb 15 - 18, 2016.

[8] W.H. Hofmeister, D.O. MacCallum, G.A. Knorovsky. “Video monitoring and control of the LENS process.” *Proceedings of the 9th International Conference of Computer Technology in Welding*, Detroit, MI, Sept. 28 - 30, 1999.

[9] D. Hu and R. Kovacevic. “Modelling and measuring the thermal behavior of the molten pool in closed-loop controlled laser-based additive manufacturing.” *Proceedings of the Institution of Mechanical Engineers, Part B: Journal of Engineering Manufacture* Vol. 217 (2003): pp. 441 - 452.

[10] D. Hu, H. Mei, G. Tao, R. Kovacevic. “Closed loop control of 3d laser cladding based on infrared sensing.” *Proceedings of the Solid Freeform Fabrication Symposium*, 2001, pp. 129 - 137.

[11] J.M. Zalameda, E.R. Burke, R.A. Hafley, K.M.B. Taminger, C.S. Domack, A. Brewer, R.E. Martin. "Thermal imaging for assessment of Electron-Beam Freeform Fabrication (EBF3) additive manufacturing deposits." *Proceedings of SPIE*, Presented in Thermosense: Thermal Infrared Applications XXXV, Vol. 8705, 2013.

[12] Michael C. Borish, Brian K. Post, Alex C. Roschli, Phillip C. Chesser, Lonnie J. Love, and Katherine T. Gaul. "Defect Identification and Mitigation via Visual Inspection in Large-Scale Additive Manufacturing." *JOM* Vol. 71 No. 3 (2019): pp. 893 - 899.

[13] Brian T. Gibson, Yashwanth K. Bandari, Bradley S. Richardson, Alex C. Roschli, Brian K. Post, Michael C. Borish, Aaron Thornton, William C. Henry, Matthew Lamsey, and Lonnie J. Love. "Melt Pool Monitoring for Control and Data Analytics in Large-Scale Metal Additive Manufacturing." *Proceedings of the Solid Freeform Fabrication Symposium* (2019): pp. 1 - 18.

[14] Brian T. Gibson, Yashwanth K. Bandari, Bradley S. Richardson, William C. Henry, Emma J. Vetland, Tayler W. Sundermann, and Lonnie J. Love. "Melt Pool Size Control Through Multiple Closed-Loop Modalities in Laser-Wire Directed Energy Deposition of Ti-6Al-4V." *Additive Manufacturing* Vol. 32 No. 3 (2020): 100993. DOI 10.1016/j.addma.2019.100993.

[15] Brian T. Gibson, Bradley S. Richardson, Tayler W. Sundermann, and Lonnie J. Love. "Beyond the Toolpath: Site-Specific Melt Pool Size Control Enables Printing of Extra-Toolpath Geometry in Laser Wire-Based Directed Energy Deposition." *Appl. Sci.* Vol. 9 No. 20 (2019): 4355. DOI 10.3390/app 9204355.